ChemComm

COMMUNICATION

View Article Online
View Journal | View Issue

Cite this: *Chem. Commun.*, 2020, **56**, 4882

Received 24th February 2020,
Accepted 2nd April 2020

DOI: 10.1039/d0cc01429j

rsc.li/chemcomm

Temperature-driven n–p conduction type switching without structural transition in a Cu-rich chalcogenide, $NaCu_5S_3$†

Shangqing Qu, [ab] Yonggang Wang, *[b] Yu Xiao, [c] Yujie Yuan,[a] Shengyi Li,[de] Jikun Chen, [a] Lidong Zhao, [c] Zhiguo Xia*[af] and Jing Zhao *[a]

We report for the first time the discovery of reversible n–p conduction type switching in a chalcogenide, $NaCu_5S_3$, without structural transition. AC impedance and first-principles simulations of the ionic migration confirmed the local melting trends of the hexagonal copper lattice at high temperatures, which could result in superionic conductivity within $NaCu_5S_3$.

There has been considerable research interest in materials with bi-stability or multi-stability, *i.e.* two or more stable or meta-stable electronic states under external stimuli such as temperature, pressure, light, and so on. Such bi-stable and multi-stable materials hold great potential in modern electronic applications such as sensors, transistors, resistive switches,[1] information storage devices,[2] *etc.* Recent research hotspots regarding bi-stable materials include the phase-change system,[3] spin-crossover,[4] metal–insulator transition,[5] and photochromism.[6,7] Representatively, Ge–Sb–Te alloys possessing controllable crystalline–amorphous phase change ability have already been widely employed in rewriteable non-volatile optical data storage systems such as compact disks (CDs), digital versatile disks (DVDs), and Blu-ray disks (BDs).[8] Another spectacular example of bi-stability is spin-crossover, in which the transition metal cations within specific metal–organic complexes exhibit dramatic low-spin to high-spin state transitions under light irradiation or temperature variation.[4,9–11]

Recently, an emerging class of semiconductors that exhibit fascinating temperature-driven conduction type switching (*i.e.* n-to-p) has been discovered, which can be operated reversibly upon temperature or voltage change near room temperature.[12–18] Currently known n–p switching compounds are limited to several Ag-based chalcogenides and halogen chalcogenides such as $Ag_{10}Te_4Br_3$,[12] AgCuS,[13,14] AgCuSe,[15,19] $AgBiSe_2$,[16] and $Tl_2Ag_{12}Se_7$,[17] and are very rare in oxide perovskites such as $Ba_xSr_{2-x}Ti_{0.8}Fe_{0.8}Nb_{0.4}O_6$.[20] Among them, $Ag_{10}Te_4Br_3$ was first reported to offer a combination of reversible conduction type switching and high silver mobility, which causes a thermopower drop of 1400 $\mu V\ K^{-1}$ during the transition. The p–n–p switching can be explained by temperature-induced polymorphism and the low-dimensional polytelluride sublattice with unexpected electrical states. Similar temperature-dependent p–n–p conduction type switching was observed in $AgBiSe_2$ and AgCuS, accompanied with reversible structural phase transitions and colossal changes of the thermopower values. It is believed that the presence of intermediate states of semimetals in these compounds is responsible for the occurrence of p–n–p transitions. Although several different theories have been proposed for the transformation of various temperature-dependent semiconductors caused by phase transitions, the exact mechanism is still being explored.

It should be noted that until now, almost all temperature-dependent conduction type switching is accompanied by structural phase transformations. Structural phase transition is supposed to result in not only electronic changes such as a change of band structure and spin states of the metal centers, but also unexpected changes of intrinsic conduction carrier types (electron or hole) *via* atomic rearrangements. In the cases of $Ag_{10}Te_4Br_3$, $AgBiSe_2$ and AgCuS, the three distinct n or p conducting states correspond to the three crystallographic polymorphs one by one, and the atomic rearrangements of the Ag–Te or Ag–Bi–Se chains are proposed to have major contributions to the conduction evolution. Therefore, firstly, it is of urgent scientific significance to explore more

[a] *The Beijing Municipal Key Laboratory of New Energy Materials and Technologies, School of Materials Sciences and Engineering, University of Science and Technology Beijing, Beijing 100083, China. E-mail: jingzhao@ustb.edu.cn, xiazg@ustb.edu.cn*
[b] *Center for High Pressure Science and Technology Advanced Research (HPSTAR), Beijing, 100094, China. E-mail: yonggang.wang@hpstar.ac.cn*
[c] *School of Materials Science and Engineering, Beihang University, Beijing 100191, China*
[d] *CAS Key Laboratory of Molecular Nanostructure and Nanotechnology, CAS Research/Education Center for Excellence in Molecular Sciences, Institute of Chemistry, Chinese Academy of Sciences (CAS), Beijing 100190, China*
[e] *School of Chemical Sciences, University of Chinese Academy of Sciences, Beijing 100049, China*
[f] *State Key Laboratory of Luminescent Materials and Devices and Institute of Optical Communication Materials, South China University of Technology, Guangzhou, 510641, China*

† Electronic supplementary information (ESI) available. See DOI: 10.1039/d0cc01429j

temperature-dependent n–p switching materials, especially those with new mechanisms. Secondly, in the currently known p–n switching materials, the switching is highly related to the intermediate phases that only exist within a narrow temperature range (*i.e.*, ~70 K of α-AgCuS, ~30 K of mixed α,β-$Ag_{10}Te_4Br_3$, and ~50 K of rhombohedral $AgBiSe_2$). Thus, it is of great practical importance to develop bi-stable n–p switching semiconductors rather than the previously reported tri-stable systems. In pursuit of novel temperature-dependent n–p switching materials, we focused on Ag- or Cu-rich chalcogenides with three-dimensional Ag/Cu sub-lattices. Such compounds always exhibit mixed ion-electron conductance at room temperature and a liquid-like behavior as temperature rises, such as AgCuS[13] and AgCuSe.[15] As a result, in these Ag- or Cu-rich systems, the transformation of conduction type is highly expected.

Here, we report the structural and physical property evolution of $NaCu_5S_3$ as a function of temperature, which shows reversible n–p conduction type switching at elevated temperatures but without any structural phase transition. This phenomenon is confirmed by means of *in situ* temperature-dependent powder X-ray diffraction, comprehensive transport measurements, and thermal analysis. Based on the AC impedance results and theoretical simulations, a new mechanism of conduction type switching in Ag- or Cu-rich chalcogenides has been proposed, which we believe will provide a reference for future exploration and structural design of novel bi-stable functional materials.

A $NaCu_5S_3$ sample was synthesized *via* a solvothermal method adopting Cu_2S, NaOH and NH_4N_2S as the raw reagents. Fig. 1a shows the room temperature powder XRD pattern of the as-obtained $NaCu_5S_3$, which confirms the high phase purity of the products as compared with the calculated peak positions.[21] The $NaCu_5S_3$ micro-crystals have a rod-like morphology and are about 30–50 μm long (Fig. S1, ESI†). The SEM images and the elemental mappings indicate good uniformity of the as-synthesized powder samples (Fig. S1, ESI†) and sintered samples (Fig. S2, ESI†). $NaCu_5S_3$ crystallizes in the space group $P6_322$ based on a hexagonal close-packed arrangement of S atoms (inset of Fig. 1a). In the crystal structure, there are two different copper sites: a Cu(1) atom coordinated with two S atoms with the same bond length of 2.186 Å, and a Cu(2) atom coordinated with three S atoms forming a regular triangular coordination environment with the Na–S bond length of 2.364 Å. Meanwhile, all the sodium atoms are located within the channels and coordinated with six S atoms forming regular octahedra with a Na–S bond length of 2.893(1) Å. $NaCu_5S_3$ is a narrow-bandgap semiconductor with the E_g value ~0.42 eV, as reported previously.[22]

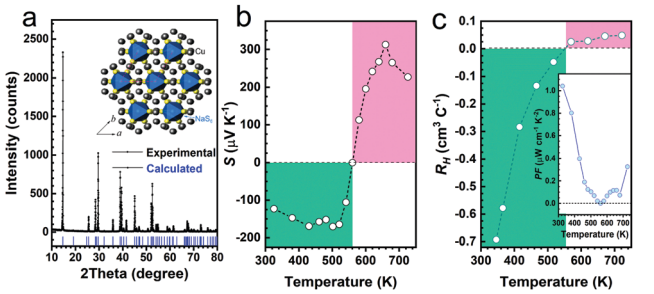

Fig. 1 (a) Powder XRD pattern of the as-synthesized $NaCu_5S_3$ sample. The inset shows the crystal structure of $NaCu_5S_3$. (b) Temperature-dependent Seebeck coefficient S and (c) Hall coefficient R_H of $NaCu_5S_3$. Obvious minus–plus sign change in both the S and the R_H can be seen, which also corresponds to the minimum value zero on the PF curve. The inset of (c) shows the power factor PF of $NaCu_5S_3$ as a function of temperature.

Fig. 1b displays the temperature dependent thermopower (S) of $NaCu_5S_3$ in the temperature range of 300–725 K. The optical images of the sample used for electrical and thermal property tests are shown in Fig. S3 (ESI†). Initially, the Seebeck coefficient of $NaCu_5S_3$ at room temperature is negative, indicating an n type conduction characteristic (*i.e.*, electron is the main carrier). As temperature increases, the S value decreases gradually from -122 μV K^{-1} at 325 K to -170 μV K^{-1} at 500 K, and then increases sharply when the temperature increases beyond 540 K. The Seebeck coefficient changes from negative to positive at around 560 K, indicating conduction type switching from n to p type. The cooling process demonstrated that when the temperature drops, the characteristic of the material changes back to n-type (Fig. S4, ESI†). Hall coefficient measurements have been conducted to confirm the n–p switching phenomenon observed from the Seebeck coefficient. The initial negative value of the Hall coefficient also represents an n type conduction behavior of $NaCu_5S_3$ at room temperature, and the positive value above 560 K represents a p type semiconducting behavior. As shown in Fig. 1c, the Hall coefficient of $NaCu_5S_3$ has a dramatic negative-to-positive transition at around 560 K, indicating the change of the main carrier from electron to hole accompanying the change in the Seebeck coefficient.

The electrical conductivity evolution (Fig. S5, ESI†) and the high Hall carrier concentration of $NaCu_5S_3$ as a function of temperature (Fig. S6, ESI†) represent the fact that $NaCu_5S_3$ is a highly degenerate semiconductor. The conductivity value decreases monotonically when the temperature increases from room temperature to 580 K and then it remains almost constant up to 680 K, which can be attributed to the competition between increased carrier concentration and phonon scattering. We also demonstrated that the change of the electrical conductivity is also reversible and repeatable (Fig. S7, ESI†). The inset of Fig. 1c represents the power factor (PF = $S^2\sigma$) of $NaCu_5S_3$ as a function of temperature. As a combination of Seebeck coefficient and electrical conductivity, the PF value of $NaCu_5S_3$ reaches zero at around 560 K accompanied with n–p switching. All this evidence proves the temperature dependent reversible n–p conduction type switching in $NaCu_5S_3$.

In general, the phenomenon of n–p conduction type switching in semiconductors is usually accompanied with the occurrence of structural phase transitions. For example, $Ag_{10}Te_4Br_3$ undergoes a $\gamma \rightarrow \beta \rightarrow \alpha$ phase transition during the p–n–p conduction type switching during a narrow temperature range: 310–410 K.[12] $AgBiSe_2$ and AgCuS undergo structural phase transitions from rhombohedral to cubic and orthorhombic to hexagonal to cubic symmetry, respectively.[13,14,16] Fig. S8 (ESI†) shows the DSC curve of synthetic $NaCu_5S_3$, which displays no obvious endothermic or exothermic peaks. The results of the TG–DTA curve of the sintered samples are consistent with this, indicating that the

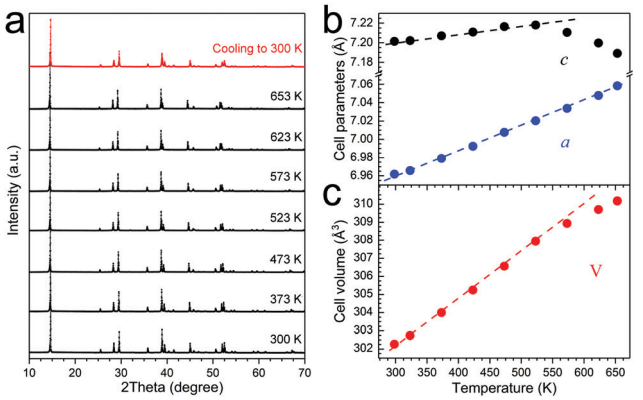

Fig. 2 (a) *In situ* temperature-dependent powder XRD patterns of $NaCu_5S_3$ during a heating/cooling cycle. (b) Cell parameters of $NaCu_5S_3$ as a function of temperature. (c) Cell volumes of $NaCu_5S_3$ as a function of temperature.

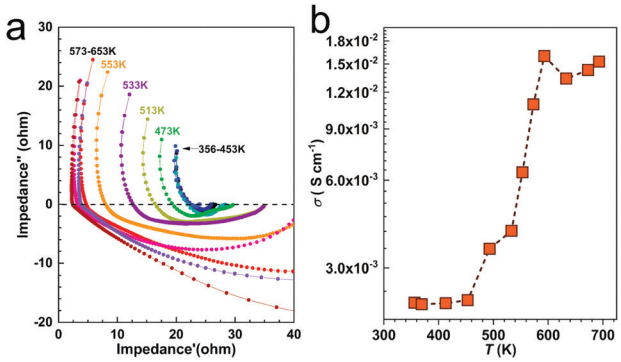

Fig. 3 (a) Impedance spectroscopy Nyquist plots of the real and imaginary components of $NaCu_5S_3$ measured at different temperatures. (b) The ionic conductivity of $NaCu_5S_3$ as a function of temperature.

structure of $NaCu_5S_3$ has excellent stability (Fig. S9, ESI†). Fig. 2a shows the *in situ* XRD measurement results of $NaCu_5S_3$ from room temperature to 653 K. Firstly, no evident phase transition can be observed as almost all of the XRD peaks remain the same but only move to lower 2θ angles, corresponding to normal lattice expansion as temperature increases. This is distinct from other known chalcogenides with temperature-dependent conduction type conversion. The underlying mechanism of the temperature-dependent n–p conduction type switching in $NaCu_5S_3$ is different from other chalcogenides. Secondly, the evolution of the powder XRD patterns during heating and cooling processes is reversible, as they return to the initial profile with almost the same cell parameters after cooling down to room temperature.

Fig. 2b shows the temperature dependence of lattice parameters derived from LeBail fitting of the powder XRD patterns. Below 523 K, the lattice parameters of both *a* and *c* increase linearly with increasing temperature. Notably, the lattice expansion along the *c*-axis deviates from the linear law above 523 K, corresponding to the occurrence of the n–p transition. This points to a subtle local structure change accompanying the conduction type switching. A reasonable speculation referring to the previous cases of superionic solid electrolytes is that the copper sublattice begins to melt locally, while the rigid sublattice of the S atom remains unchanged.

The ionic conductivity of $NaCu_5S_3$ was measured using the 6w?>AC impedance method. Fig. 3a shows the representative Nyquist plots for $NaCu_5S_3$ from room temperature to 653 K. At temperatures lower than 533 K, most of the impedance plots are composed of two partially overlapped semicircles corresponding to the separate contributions from the bulk particles and grain boundaries. As temperature further increases, the two semicircles gradually tend to be spike-like, indicating the greatly increased ionic conduction in $NaCu_5S_3$ and the combined component of inductance. The total ionic conductivities were calculated based on the intercept to the real axis, and the result is shown in Fig. 3b. Notably, the ionic conductivity rises rapidly in the temperature range of 500–600 K, from $\sim 3.5 \times 10^{-3}$ S cm^{-1} to $\sim 15.0 \times 10^{-3}$ S cm^{-1}. This can be attributed to the local melting of the copper sublattice by comparing to the similar behavior of PbF_2, CaF_2 and $Cu_{2-x}Se$.[23–25] High copper ionic mobility or even a liquid-like copper sublattice has been observed in a collection of copper themoelectrics.[26–32] Considering the absence of structural phase transition, one has reasons to believe that the melting of the copper sublattice is closely related to the n–p type conduction switching in $NaCu_5S_3$. It is also notable that the overall ionic conductivity of $NaCu_5S_3$ reflected from the AC impedance spectra is very complex, and at least consists of the contributions from Na^+ ions, Cu^+ ions and electronic conductivity involving both electrons and holes.

To gain more insights into the superionic conductivity and copper sublattice melting in $NaCu_5S_3$, we performed a DFT simulation to evaluate the migration of monovalent cations Na^+ and Cu^+ within the $NaCu_5S_3$ structure. Fig. 4a shows the sublattice of Na^+ and Cu^+ cations, in which two distinct Cu atoms can be observed and all the Na atoms locate in the same chemical environment forming a one-dimensional chain along the *c*-axis. Firstly, we can check the atomic distances of Cu1–Cu1, Cu2–Cu2 and Na1–Na1 of 3.78 Å, 3.26 Å and 3.60 Å, respectively. The closest atomic distance is between Cu1 and Cu2, and is only 2.71 Å. Such a small distance is beneficial to reduce the migration barrier between Cu1 and Cu2, thereby facilitating the migration between Cu1 and Cu2. Fig. 4b provides the calculated cation migration barrier from one cation site to the nearest one: ~1.8 eV for Cu1–Cu1, ~1.7 eV for Cu2–Cu2, ~0.9 eV for Na1–Na1 and ~0.4 eV for Cu1–Cu2, respectively. This result indicates that compared to the other three possibilities, the migration within Cu1–Cu2 sites requires the least active energy. Thus, local melting will very likely occur within the copper sublattice and is specifically related to the Cu1–Cu2 interposition migration. The copper sublattice melting at elevated temperatures not only provides superionic conductivity but also results in dramatic conduction type switching.

In summary, we synthesized a Cu-rich chalcogenide semiconductor, $NaCu_5S_3$, using a facile hydrothermal method. The material exhibits a reversible temperature-driven n-to-p conduction type transition at around 560 K but without any structural phase transition, which is distinct from all the p–n–p switching chalcogenides reported so far. By a combination of comprehensive

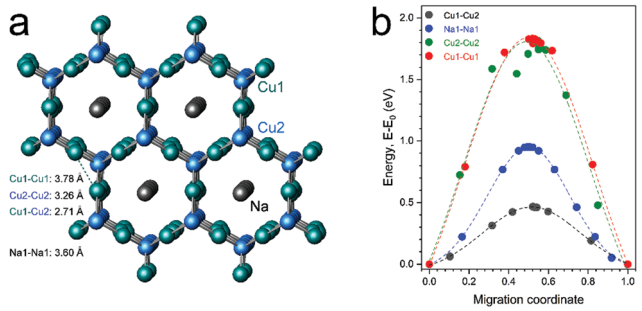

Fig. 4 (a) Schematic representation of the atomic arrangement of the copper sublattice within the $NaCu_5S_3$ structure. (b) The energies required for cation migration in $NaCu_5S_3$. The four most possible migration paths are compared, with the Cu1–Cu2 diffusion path giving the minimal energy.

experimental characterization methods of *in situ* temperature-dependent powder XRD, Seebeck and Hall coefficient analysis, AC impedance analysis and DFT calculations, we demonstrate that the temperature-dependent n–p switching in $NaCu_5S_3$ is driven by copper sublattice melting. The discovery of this new mechanism bridges functional semiconducting materials and superionic solid electrolytes. Compared with common p- or n-type semiconductors and p–n junctions made from them,[33] temperature-dependent p–n switching materials show potential in the concept of "dual-control" either by external environments or by artificial operations. We believe that future exploration of ionic conducting materials with order–disorder transitions or sublattice melting behaviors will provide more temperature-dependent conduction type switching materials.

Conflicts of interest

There are no conflicts to declare.

Notes and references

1 M. Andrzejewski and A. Katrusiak, *J. Phys. Chem. Lett.*, 2017, **8**, 929–935.
2 M. Wuttig and N. Yamada, *Nat. Mater.*, 2007, **6**, 824–832.
3 N. Yamada, E. Ohno, N. Akahira, K. I. Nishiuchi, K. I. Nagata and M. Takao, *Jpn. J. Appl. Phys.*, 1987, **26**, 61.
4 J.-B. Lin, W. Xue, B.-Y. Wang, J. Tao, W.-X. Zhang, J.-P. Zhang and X.-M. Chen, *Inorg. Chem.*, 2012, **51**, 9423–9430.
5 G. J. Hyland, *J. Solid State Chem.*, 1970, **2**, 318–331.
6 P.-X. Li, M.-S. Wang, M.-J. Zhang, C.-S. Lin, L.-Z. Cai, S.-P. Guo and G.-C. Guo, *Angew. Chem., Int. Ed.*, 2014, **53**, 11529–11531.
7 J.-J. Shen, X.-X. Li, T.-L. Yu, F. Wang, P.-F. Hao and Y.-L. Fu, *Inorg. Chem.*, 2016, **55**, 8271–8273.
8 N. Yamada, E. Ohno, K. Nishiuchi, N. Akahira and M. Takao, *J. Appl. Phys.*, 1991, **69**, 2849–2856.
9 B. Weber, W. Bauer and J. Obel, *Angew. Chem., Int. Ed.*, 2008, **47**, 10098–10101.
10 G. J. Halder, C. J. Kepert, B. Moubaraki, K. S. Murray and J. D. Cashion, *Science*, 2002, **298**, 1762.
11 J. J. Scepaniak, T. D. Harris, C. S. Vogel, J. Sutter, K. Meyer and J. M. Smith, *J. Am. Chem. Soc.*, 2011, **133**, 3824–3827.
12 T. Nilges, S. Lange, M. Bawohl, J. M. Deckwart, M. Janssen, H.-D. Wiemhöfer, R. Decourt, B. Chevalier, J. Vannahme, H. Eckert and R. Weihrich, *Nat. Mater.*, 2009, **8**, 101.
13 S. N. Guin, J. Pan, A. Bhowmik, D. Sanyal, U. V. Waghmare and K. Biswas, *J. Am. Chem. Soc.*, 2014, **136**, 12712–12720.
14 M. Dutta, D. Sanyal and K. Biswas, *Inorg. Chem.*, 2018, **57**, 7481–7489.
15 C. Han, Q. Sun, Z. X. Cheng, J. L. Wang, Z. Li, G. Q. Lu and S. X. Dou, *J. Am. Chem. Soc.*, 2014, **136**, 17626–17633.
16 C. Xiao, X. Qin, J. Zhang, R. An, J. Xu, K. Li, B. Cao, J. Yang, B. Ye and Y. Xie, *J. Am. Chem. Soc.*, 2012, **134**, 18460–18466.
17 Y. Shi, A. Assoud, C. R. Sankar and H. Kleinke, *Chem. Mater.*, 2017, **29**, 9565–9571.
18 S. N. Guin and K. Biswas, *Phys. Chem. Chem. Phys.*, 2015, **17**, 10316–10325.
19 S. Ishiwata, Y. Shiomi, J. S. Lee, M. S. Bahramy, T. Suzuki, M. Uchida, R. Arita, Y. Taguchi and Y. Tokura, *Nat. Mater.*, 2013, **12**, 512.
20 P. Roy, V. Waghmare, K. Tanwar and T. Maiti, *Phys. Chem. Chem. Phys.*, 2017, **19**, 5818–5829.
21 H. Effenberger and F. Pertlik, *Monatsh. Chem.*, 1985, **116**, 921.
22 W. Bu-Yong, Y. Jin-She, F. Qing and W. Ao, *Acta Phys. Sin.*, 2013, **62**, 178102.
23 J. B. Boyce, J. C. Mikkelsen and M. O'Keeffe, *Solid State Commun.*, 1977, **21**, 955–958.
24 S. E. Boulfelfel, D. Zahn, O. Hochrein, Y. Grin and S. Leoni, *Phys. Rev. B: Condens. Matter Mater. Phys.*, 2006, **74**, 094106.
25 H. Liu, X. Shi, F. Xu, L. Zhang, W. Zhang, L. Chen, Q. Li, C. Uher, T. Day and G. J. Snyder, *Nat. Mater.*, 2012, **11**, 422–425.
26 K. Zhao, A. B. Blichfeld, H. Chen, Q. Song, T. Zhang, C. Zhu, D. Ren, R. Hanus, P. Qiu, B. B. Iversen, F. Xu, G. J. Snyder, X. Shi and L. Chen, *Chem. Mater.*, 2017, **29**, 6367–6377.
27 Y. He, T. Day, T. Zhang, H. Liu, X. Shi, L. Chen and G. J. Snyder, *Adv. Mater.*, 2014, **26**, 3974–3978.
28 H. Liu, X. Yuan, P. Lu, X. Shi, F. Xu, Y. He, Y. Tang, S. Bai, W. Zhang, L. Chen, Y. Lin, L. Shi, H. Lin, X. Gao, X. Zhang, H. Chi and C. Uher, *Adv. Mater.*, 2013, **25**, 6607–6612.
29 P. Qiu, X. Shi and L. Chen, *Energy Storage Mater.*, 2016, **3**, 85–97.
30 J. Zhang, R. Liu, N. Cheng, Y. Zhang, J. Yang, C. Uher, X. Shi, L. Chen and W. Zhang, *Adv. Mater.*, 2014, **26**, 3848–3853.
31 K. Zhao, P. Qiu, Q. Song, A. B. Blichfeld, E. Eikeland, D. Ren, B. Ge, B. B. Iversen, X. Shi and L. Chen, *Mater. Today Phys.*, 2017, **1**, 14–23.
32 K. S. Weldert, W. G. Zeier, T. W. Day, M. Panthöfer, G. J. Snyder and W. Tremel, *J. Am. Chem. Soc.*, 2014, **136**, 12035–12040.
33 P. K. Sahoo, S. Memaran, Y. Xin, L. Balicas and H. R. Gutiérrez, *Nature*, 2018, **553**, 63–67.